

Elastic/plastic buckling analysis of skew plates under in-plane shear loading with incremental and deformation theories of plasticity by GDQ method

M. Maarefdoust & M. Kadkhodayan

**Journal of the Brazilian Society of
Mechanical Sciences and Engineering**

ISSN 1678-5878
Volume 37
Number 2

J Braz. Soc. Mech. Sci. Eng. (2015)
37:761-776
DOI 10.1007/s40430-014-0203-6



Your article is protected by copyright and all rights are held exclusively by The Brazilian Society of Mechanical Sciences and Engineering. This e-offprint is for personal use only and shall not be self-archived in electronic repositories. If you wish to self-archive your article, please use the accepted manuscript version for posting on your own website. You may further deposit the accepted manuscript version in any repository, provided it is only made publicly available 12 months after official publication or later and provided acknowledgement is given to the original source of publication and a link is inserted to the published article on Springer's website. The link must be accompanied by the following text: "The final publication is available at link.springer.com".

Elastic/plastic buckling analysis of skew plates under in-plane shear loading with incremental and deformation theories of plasticity by GDQ method

M. Maarefdoust · M. Kadkhodayan

Received: 18 January 2014 / Accepted: 2 June 2014 / Published online: 22 June 2014
© The Brazilian Society of Mechanical Sciences and Engineering 2014

Abstract The present study is concerned with the elastic/plastic buckling analysis of a skew plate under in-plane shear loading. The governing equations for moderately thick skew plates are analytically derived based on first-order shear deformation theory, whereas the incremental and deformation theories of plasticity are employed. Two types of shear loads, i.e. rectangular shear (R-shear) and skew shear (S-shear) have been investigated. The buckling coefficient values are significantly affected by the direction of stresses. Since the problem is geometrically and physically nonlinear, the generalized differential quadrature method as an accurate, simple and computationally efficient numerical tool is adopted to discretize the governing equations and the related boundary conditions. Then, a direct iterative method is employed to obtain the buckling coefficients of skew plates. To demonstrate the accuracy of the present analytical solution, a comparison is made with the published experimental and numerical results in literature. The influences of the aspect and thickness ratios, skew angle, incremental and deformation theories and various boundary conditions are examined for R-shear and S-shear buckling coefficients. Finally, some mode shapes of the skew thick plates are illustrated. The present results may serve as benchmark solutions for such plates.

Keywords Incremental theory (IT) · Skew plate · GDQM · Deformation theory (DT) · Elastic/plastic buckling · FSDT

List of symbols

a	Length of plate
$A_{ij}^{\xi}, A_{ij}^{\eta}$	Weighting coefficients of the first-order derivative in ξ - and η -directions, respectively
b	Oblique width of plate
$B_{ij}^{\xi}, B_{ij}^{\eta}$	Weighting coefficients of the second-order derivative in ξ - and η -directions, respectively
c, k	Ramberg–Osgood parameters
D	Flexural rigidity of plate
E	Young's modulus of elasticity
G	Effective shear modulus
h	Thickness of plate
h/b	Thickness ratio
N_{ξ}, N_{η}	Number of grid points in ξ - and η -directions, respectively
S_{ij}	Stress deviator tensor
$S(E_s)$	Secant modulus
$T(E_t)$	Tangent modulus
U	Strain energy
V	Potential energy
W_{ij}	Deflection at grid point ij
X_i	Grid spacing
x, y, z	The Cartesian coordinate variables

Greek symbols

$\alpha, \beta, \gamma, \chi, \mu, \delta$	Parameters used in stress–strain relations
ϵ_e	Total effective strain
ϵ	Total plastic strain
$\epsilon_x, \epsilon_y, \epsilon_{xy}$	Normal strain
$\varphi_x, \varphi_y, \varphi_{\xi}, \varphi_{\eta}$	Rotations about x -, y -, ξ and η

Technical Editor: Lavinia Maria Sanabio Alves Borges.

M. Maarefdoust · M. Kadkhodayan (✉)
Department of Mechanical Engineering, Ferdowsi University of
Mashhad, 91775-1111 Mashhad, Iran
e-mail: kadkhoda@um.ac.ir

M. Maarefdoust
e-mail: m_maarefdoost@yahoo.com

κ^2	Shear correction factor
λ_{xy}	Elastic/plastic shear buckling coefficient
λ_R	Elastic/plastic buckling coefficient for R-shear loading
λ_S	Elastic/plastic buckling coefficient for S-shear loading
ν	Poisson's ratio
θ	Skew angle
σ_e	Effective stress
$\sigma_x, \sigma_y, \sigma_{xy}$	Normal stress
ξ, η	Oblique coordinate variables

1 Introduction

Skew plates under shear loading have found considerable applications in structural engineering problems. Aircraft wings and skew bridges are well-known direct applications of these kinds of plates. The elastic buckling of skew plates has been studied by some researchers [1–3]. However, to the best of author's knowledge, the plastic buckling of skew plates is not available in open literature. There are many such kind methods available, such as Rayleigh–Ritz, finite element, finite difference and Fourier series methods. Rayleigh–Ritz and Fourier series methods require less computational effort as compared with finite element and finite difference methods. Some researchers studied elastic/plastic buckling of rectangular plates [4–9]. By contrast, no results exist for elastic/plastic shear buckling of skew plates. Moreover, the discrepancies between the incremental and deformation theories results in skew plates have not been studied.

Two types of shear loading conditions on skew plates are considered, i.e. (a) R-shear loading and (b) S-shear loading, Fig. 1. The first type is the shear loading acting along the two horizontal edges and the traction is a pure shear stress, whereas along the other two oblique edges, the traction consists of both shear and direct stresses of such magnitude that every infinitesimal rectangular element is in a state of pure shear, Fig. 1a. The second type is the shear loads are uniformly applied along the plate edges, Fig. 1b. For the R-shear loading, we have $\sigma_x = 0$ and $\tau_{xy} = R$, while for S-shear loading $\sigma_x = -2S \tan(\theta)$ and $\tau_{xy} = S$. The positive and negative angle values are defined in clockwise and anticlockwise directions, respectively. The main difference between the shear buckling of skew and rectangular plates is that a reversal of the direction of the shear loading will not cause a change in the critical shear load value for rectangular plates whereas it will affect the critical shear load in skew plates [10].

The first studies on elastic shear buckling of skew plate performed by Wittrick [11]. He solved the elastic buckling problem of simply supported and clamped skew plates under pure shear. Argyris [12], Ashton [13], Durvasula [14,

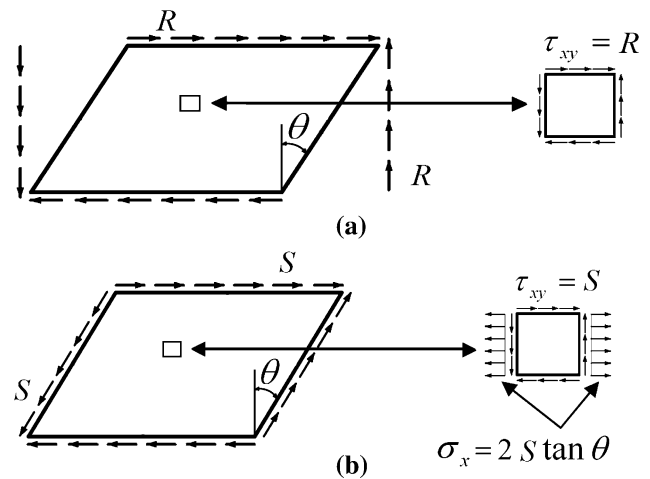


Fig. 1 Two types of shear loading conditions on skew plates, **a** R-shear loading and **b** S-shear loading

15], Xiang et al. [16] and York [17] performed elastic R-shear buckling of skew plates and Hamada [18], Fried and Schmitt [19], Yoshimura and Iwata [20] and Xiang et al. [16] studied elastic S-shear buckling of skew plates.

The plastic buckling analyses of rectangular plates by incremental and deformation theories of plasticity and subjected to in-plane loadings have been studied in the past several decades. Durban [21] studied on the plastic buckling of rectangular plates. He found that the incremental theory predicts more buckling load than deformation theory, and the experimental data have more congruence with the deformation theory. Durban and Zuckerman [22] carried out the plastic buckling analyses of rectangular plates under uniaxial loading for several various modes with the separation of variables solution. However, their boundary conditions were limited to clamped and simply supported types. Wang et al. [23, 24] investigated the elastic–plastic buckling of thin and thick plates based on deformation and incremental theories by use of separation of variables solution and Ritz method. They came to the conclusion that the deformation theory predicts a lower buckling stress factor, and as the thickness increases and hardening decreases (Ramberg–Osgood constant increases), the differences between the two theories increase. Lotfi et al. [25] analyzed a skew isotropic plate subjected to in-plane loadings using a stability analysis based on the isoparametric spline finite strip method that includes inelasticity. The stiffness and stability matrices were formulated by energy expressions using small deflection theory. Jaberzadeh et al. [26] analyzed the plastic buckling of thin skew plates using element-free Galerkin (EFG) method. They used Stowell theory for the plastic buckling of skew plates with variable thickness and concluded that the plastic critical stresses increased with increasing the thickness of the plate. Zhang and Wang [8] confirmed the reported results given by Ref. [23]. Kadkhodayan and Maa-refdoust [9] studied the elastic/plastic buckling of thin

rectangular plates under various loads and boundary conditions. To the best knowledge of the authors, there is no solution available in the open literature for plastic buckling analysis of skew plates under R-shear and S-shear loading.

In the current study, the differential equations of elastic/plastic buckling of skew plates are derived and the GDQ method is used for solving those equations. The formulation is based on first-order shear deformation theory (FSDT) and the incremental and deformation theories of plasticity are used. Two shear loading conditions containing R- and S-shear loadings are studied. Results are compared with existing data available from other analytical and numerical methods. The effects of skew plate parameters such as aspect and thickness ratios, skew angles, incremental and deformation theories and boundary conditions on the R- and S-shear buckling coefficients are presented. Finally, some plots of the mode shapes are illustrated for the R- and S-shear buckling.

2 Mathematical formulations

2.1 Governing differential equations

Let us consider a skew moderately thick plate with length a , oblique width b , thickness h and skew angle θ as shown in Fig. 2. The stress rate corresponding to strain rate in Cartesian coordinate are given by

$$\begin{aligned} \dot{\sigma}_x &= E(\alpha\dot{\epsilon}_x + \beta\dot{\epsilon}_y + \chi\dot{\gamma}_{xy}), \\ \dot{\sigma}_y &= E(\beta\dot{\epsilon}_x + \gamma\dot{\epsilon}_y + \mu\dot{\gamma}_{xy}), \\ \dot{\tau}_{xy} &= E(\chi\dot{\epsilon}_x + \mu\dot{\epsilon}_y + \delta\dot{\gamma}_{xy}), \\ \dot{\tau}_{xz} &= \kappa^2 G\dot{\gamma}_{xz}, \quad \dot{\tau}_{yz} = \kappa^2 G\dot{\gamma}_{yz}, \end{aligned} \tag{1}$$

where E is the Young modulus, G is the shear modulus, κ^2 is the shear correction factor and $\alpha, \beta, \gamma, \chi, \mu, \delta$ and G depend on theories of plasticity used. There are two theories of plasticity used in this paper, the incremental theory based on Prandtl-Reuss equation and the deformation theory based on Hencky equation. In the current study, the first shear deformation theory which is suitable for

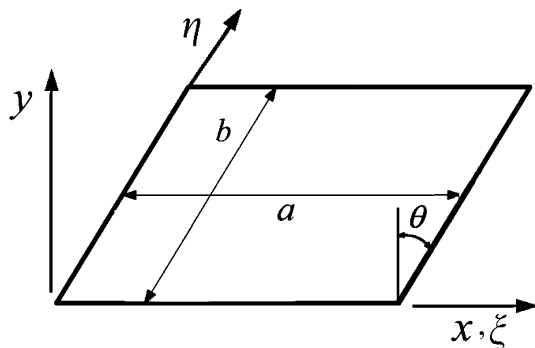


Fig. 2 The geometry of the skew plate

moderately thick plates is employed. The main difference between these two is that the IT depends on incremental plastic strain and DT depends on total strain. The strain-displacement relations can be expressed as

$$\begin{aligned} \epsilon_x &= z \frac{\partial \varphi_x}{\partial x}, \quad \epsilon_y = z \frac{\partial \varphi_y}{\partial y}, \\ \gamma_{xy} &= z \left(\frac{\partial \varphi_x}{\partial y} + \frac{\partial \varphi_y}{\partial x} \right), \quad \gamma_{xz} = \varphi_x + \frac{\partial w}{\partial x}, \quad \gamma_{yz} = \varphi_y + \frac{\partial w}{\partial y}, \end{aligned} \tag{2}$$

where w is transverse displacement and φ_x, φ_y denote the rotations of the transverse normal about x - and y -axis, respectively. The strain energy functional for the plate is given by

$$U = \frac{1}{2} \int_V \{ \dot{\sigma}_x \dot{\epsilon}_x + \dot{\sigma}_y \dot{\epsilon}_y + \dot{\tau}_{xy} \dot{\gamma}_{xy} + \dot{\tau}_{xz} \dot{\gamma}_{xz} + \dot{\tau}_{yz} \dot{\gamma}_{yz} \} dV. \tag{3}$$

The potential energy V for the plate subjected to uniform in-plane stress is given by

$$V = -\frac{1}{2} \int_A \left[\sigma_x h \left(\frac{\partial w}{\partial x} \right)^2 + \sigma_y h \left(\frac{\partial w}{\partial y} \right)^2 + 2\tau_{xy} h \left(\frac{\partial w}{\partial x} \right) \left(\frac{\partial w}{\partial y} \right) \right] dA. \tag{4}$$

The principle of minimum total potential energy is $\delta(U + V) = 0$,

where δ represent the variational symbol. The material points of skew plates in the physical domain can be transformed into computational domain of the GDQM, which is a rectangular one, without any approximation using the following linear transformation rules

$$\begin{aligned} x &= \xi + \eta(\sin \theta), \\ y &= \eta(\cos \theta), \end{aligned} \tag{6}$$

where ξ and η are natural coordinate variables of the computational domain and θ is the skew angle. The rotations φ_x, φ_y can be expressed in the skew coordinate system as

$$\begin{aligned} \varphi_x(x, y) &= \varphi_\xi(\xi, \eta) \cos \theta, \\ \varphi_y(x, y) &= -\varphi_\xi(\xi, \eta) \sin \theta + \varphi_\eta(\xi, \eta). \end{aligned} \tag{7}$$

The fundamental equation of incremental theory with Prandtl-Reuss constitutive equation is [23]

$$E\dot{\epsilon}_{ij} = (1 + \nu)\dot{S}_{ij} + \frac{1 - 2\nu}{3}\dot{\sigma}_{kk}\delta_{ij} + \frac{3\dot{\sigma}_e}{2\sigma_e} \left(\frac{E}{T} - 1 \right) S_{ij}, \tag{8}$$

where T is the tangent modulus which is calculated through stress-strain curved and σ_e is the effective stress. The tangent modulus and effective stress are calculated as follow:

$$\begin{aligned} T &= d\sigma_e/d\epsilon_e, \\ \sigma_e^2 &= \sigma_x^2 - \sigma_x\sigma_y + \sigma_y^2 + 3\tau_{xy}^2, \end{aligned} \tag{9}$$

where ε_e is the total effective strain. The parameters $\alpha, \beta, \gamma, \chi, \mu, \delta$ and G in this method are defined as

$$\begin{aligned} \alpha &= \frac{1}{\rho} [c_{22}c_{33} - c_{23}^2], & \beta &= \frac{1}{\rho} [c_{13}c_{23} - c_{12}c_{33}], \\ \gamma &= \frac{1}{\rho} [c_{11}c_{33} - c_{13}^2], \\ \mu &= \frac{1}{\rho} [c_{12}c_{13} - c_{11}c_{23}], & \chi &= \frac{1}{\rho} [c_{12}c_{23} - c_{13}c_{22}], \\ \delta &= \frac{1}{\rho} [c_{11}c_{22} - c_{12}^2], \\ \rho &= \frac{E}{T} \begin{vmatrix} c_{11} & c_{12} & c_{13} \\ c_{21} & c_{22} & c_{23} \\ c_{31} & c_{32} & c_{33} \end{vmatrix}, & G &= \frac{E}{2(1+\nu)}, \end{aligned} \tag{10}$$

in which

$$\begin{aligned} c_{11} &= 1 - 3 \left(1 - \frac{T}{E}\right) \left(\frac{\sigma_y^2}{4\sigma_e^2} + \frac{\tau_{xy}^2}{\sigma_e^2}\right), \\ c_{12} &= -\frac{1}{2} \left[1 - (1 - 2\nu) \frac{T}{E} - 3 \left(1 - \frac{T}{E}\right) \left(\frac{\sigma_x \sigma_y}{2\sigma_e^2} + \frac{\tau_{xy}^2}{\sigma_e^2}\right)\right], \\ c_{13} &= \frac{3}{2} \left(1 - \frac{T}{E}\right) \left(\frac{2\sigma_x - \sigma_y}{\sigma_e}\right) \left(\frac{\tau_{xy}}{\sigma_e}\right), \\ c_{22} &= 1 - 3 \left(1 - \frac{T}{E}\right) \left(\frac{\sigma_x^2}{4\sigma_e^2} + \frac{\tau_{xy}^2}{\sigma_e^2}\right), \\ c_{23} &= \frac{3}{2} \left(1 - \frac{T}{E}\right) \left(\frac{2\sigma_y - \sigma_x}{\sigma_e}\right) \left(\frac{\tau_{xy}}{\sigma_e}\right), \\ c_{33} &= 2(1 + \nu) \left(\frac{T}{E}\right) + 9 \left(1 - \frac{T}{E}\right) \left(\frac{\tau_{xy}^2}{\sigma_e^2}\right). \end{aligned} \tag{11}$$

The fundamental equation of deformation theory with Hencky constitutive equation is [23]

$$E\dot{\varepsilon}_{ij} = \left(\frac{3E}{2S} - \frac{1-2\nu}{2}\right) \dot{S}_{ij} + \frac{1-2\nu}{3} \dot{\sigma}_{kk} \delta_{ij} + \frac{3\dot{\sigma}_e}{2\sigma_e} \left(\frac{E}{T} - \frac{E}{S}\right) S_{ij}, \tag{12}$$

where S is the secant modulus which is calculated through stress–strain uniaxial curve. The parameters $\alpha, \beta, \gamma, \chi, \mu$, and δ are calculated using Eq. (10), and G in this theory is given by

$$G = \frac{E}{2 + 2\nu + 3\left(\frac{E}{S} - 1\right)}, \tag{13}$$

in which

$$\begin{aligned} c_{11} &= 1 - 3 \left(1 - \frac{T}{S}\right) \left(\frac{\sigma_y^2}{4\sigma_e^2} + \frac{\tau_{xy}^2}{\sigma_e^2}\right), \\ c_{12} &= -\frac{1}{2} \left[1 - (1 - 2\nu) \frac{T}{E} - 3 \left(1 - \frac{T}{S}\right) \left(\frac{\sigma_x \sigma_y}{2\sigma_e^2} + \frac{\tau_{xy}^2}{\sigma_e^2}\right)\right], \end{aligned}$$

$$\begin{aligned} c_{13} &= \frac{3}{2} \left(1 - \frac{T}{S}\right) \left(\frac{2\sigma_x - \sigma_y}{\sigma_e}\right) \left(\frac{\tau_{xy}}{\sigma_e}\right), \\ c_{22} &= 1 - 3 \left(1 - \frac{T}{S}\right) \left(\frac{\sigma_x^2}{4\sigma_e^2} + \frac{\tau_{xy}^2}{\sigma_e^2}\right), \\ c_{23} &= \frac{3}{2} \left(1 - \frac{T}{S}\right) \left(\frac{2\sigma_y - \sigma_x}{\sigma_e}\right) \left(\frac{\tau_{xy}}{\sigma_e}\right), \\ c_{33} &= 3 \frac{T}{S} - (1 - 2\nu) \left(\frac{T}{E}\right) + 9 \left(1 - \frac{T}{S}\right) \left(\frac{\tau_{xy}^2}{\sigma_e^2}\right). \end{aligned} \tag{14}$$

It can be notified that by setting $T = S = E$, the parameters $\alpha, \beta, \gamma, \chi, \mu$, and δ reduce to the parameters for elastic buckling. Using Eqs. (1)–(7) and calculus of variations, the Euler–Lagrange differential equations associated with the minimization of the total potential energy functional, the equilibrium equation of elastic/plastic buckling of skew thick plate can be derived.

2.2 Discretization of governing equations

Employing the chain rule for the spatial derivatives and coordinate transformation in Eq. (6), the derivatives in this domain are expressed in terms of derivatives of space variables of the computational domains. Simultaneously, the GDQ discretization rules can be used to discretize the spatial derivatives in the computational domain [27–29]. After that, the GDQ-discretized form of the equations of elastic/plastic buckling of skew plates at each grid point (i, j) , with $i = 2, 3, \dots, N_\xi - 1$ and $j = 2, 3, \dots, N_\eta - 1$ become

$$\begin{aligned} &\left[-(\sec \theta) \sum_{m=1}^{N_\xi} A_{im}^\xi \varphi_{mj}^\xi + (\tan \theta) \sum_{m=1}^{N_\xi} A_{im}^\xi \varphi_{mj}^\eta \right. \\ &- (\sec^2 \theta) \sum_{m=1}^{N_\xi} B_{im}^\xi w_{mj} - (\sec^2 \theta) \sum_{n=1}^{N_\eta} B_{jn}^\eta w_{in} \\ &+ (2 \tan \theta \sec \theta) \sum_{m=1}^{N_\xi} \sum_{n=1}^{N_\eta} A_{im}^\xi A_{jn}^\eta w_{mn} \\ &- (\sec \theta) \sum_{n=1}^{N_\eta} A_{jn}^\eta \varphi_{in}^\eta + (\tan \theta) \sum_{n=1}^{N_\eta} A_{jn}^\eta \varphi_{in}^\xi \left. \right] k^2 Gh \cos \theta \\ &- \sigma_x h \left[(\cos \theta) \sum_{m=1}^{N_\xi} B_{im}^\xi w_{mj} \right] \\ &- \sigma_y h \left[(\tan \theta \sin \theta) \sum_{m=1}^{N_\xi} B_{im}^\xi w_{mj} - (2 \tan \theta) \sum_{m=1}^{N_\xi} \sum_{n=1}^{N_\eta} A_{im}^\xi A_{jn}^\eta w_{mn} \right. \\ &+ (\sec \theta) \sum_{n=1}^{N_\eta} B_{jn}^\eta w_{in} \left. \right] \\ &- 2\tau_{xy} h \left[\sum_{m=1}^{N_\xi} \sum_{n=1}^{N_\eta} A_{im}^\xi A_{jn}^\eta w_{mn} - (\sin \theta) \sum_{m=1}^{N_\xi} B_{im}^\xi w_{mj} \right] \\ &= 0, \end{aligned} \tag{15}$$

Table 1 Accuracy of grid points distribution for CCCC skew plate ($h/b = 0.001$, $\theta = +45^\circ$, $N_\xi = N_\eta = 13$)

Source	Shear buckling coefficient	Theories of plasticity	Eq. (B.5)	Eq. (B.4)	Eq. (B.3)	Eq. (B.2)	Eq. (B.1)
Xiang et al. [16]	$\lambda_R = 24.04$						
Present study	λ_R	IT, DT	24.040	24.027	23.981	23.997	24.027
Xiang et al. [16]	$\lambda_S = 89.16$						
Present study	λ_S	IT, DT	89.163	89.171	89.132	89.135	89.183

$$\begin{aligned}
 & \left[\frac{\alpha Eh^3}{12} \cos^3 \theta + \frac{Eh^3}{12} (2\beta + 4\delta) \sin^2 \theta \cos \theta + \frac{Eh^3}{12} (\gamma \tan \theta - 4\mu) \sin^3 \theta \right. \\
 & \left. - 4 \frac{\chi Eh^3}{12} \cos^2 \theta \sin \theta \right] \left[\sum_{m=1}^{N_\xi} B_{im}^\xi \varphi_{mj}^\xi \right] + \left[\mu - \frac{\gamma Eh^3}{12} \tan \theta \right] \left[\sum_{n=1}^{N_\eta} B_{jn}^\eta \varphi_{in}^\eta \right] \\
 & - \left[\frac{Eh^3}{12} (\beta + 2\delta) \sin \theta \cos \theta + \frac{Eh^3}{12} (\gamma \tan \theta - 3\mu) \sin^2 \theta - \frac{\chi Eh^3}{12} \cos^2 \theta \right] \left[\sum_{m=1}^{N_\xi} B_{im}^\xi \varphi_{mj}^\eta \right] \\
 & - \left[2 \frac{Eh^3}{12} (\beta + 2\delta) \cos \theta \sin \theta + 2 \frac{Eh^3}{12} (\gamma \tan \theta - 3\mu) \sin^2 \theta - 2 \frac{\chi Eh^3}{12} \cos^2 \theta \right] \tag{16}
 \end{aligned}$$

$$\begin{aligned}
 & \times \left[\sum_{m=1}^{N_\xi} \sum_{n=1}^{N_\eta} A_{im}^\xi A_{jn}^\eta \varphi_{mn}^\xi \right] + \left[\frac{Eh^3}{12} (\gamma \tan \theta - 2\mu) \sin \theta + \frac{\delta Eh^3}{12} \cos \theta \right] \left[\sum_{n=1}^{N_\eta} B_{jn}^\eta \varphi_{in}^\xi \right] \\
 & + \left[\frac{Eh^3}{12} (\beta + \delta) \cos \theta + 2 \frac{Eh^3}{12} (\gamma \tan \theta - 2\mu) \sin \theta \right] \left[\sum_{m=1}^{N_\xi} \sum_{n=1}^{N_\eta} A_{im}^\xi A_{jn}^\eta \varphi_{mn}^\eta \right] \\
 & - k^2 Gh \cos \theta \left[\varphi_{ij}^\xi - (\sin \theta) \varphi_{ij}^\eta + (\sec \theta) \sum_{m=1}^{N_\xi} A_{im}^\xi w_{mj} - (\tan \theta) \sum_{n=1}^{N_\eta} A_{jn}^\eta w_{in} \right] = 0,
 \end{aligned}$$

$$\begin{aligned}
 & \left[-\frac{Eh^3}{12} (\beta + 2\delta) \sin \theta \cos \theta - \frac{Eh^3}{12} (\gamma \tan \theta - 3\mu) \sin^2 \theta + \frac{\chi Eh^3}{12} \cos^2 \theta \right] \left[\sum_{m=1}^{N_\xi} B_{im}^\xi \varphi_{mj}^\xi \right] \\
 & + \left[\frac{Eh^3}{12} (\gamma \tan \theta - 2\mu) \sin \theta + \frac{\delta Eh^3}{12} \cos \theta \right] \left[\sum_{m=1}^{N_\xi} B_{im}^\xi \varphi_{mj}^\eta \right] + \left[\frac{\gamma Eh^3}{12} \sec \theta \right] \left[\sum_{n=1}^{N_\eta} B_{jn}^\eta \varphi_{in}^\eta \right] \\
 & + \left[2 \frac{Eh^3}{12} (\gamma \tan \theta - 2\mu) \sin \theta + \frac{Eh^3}{12} (\delta + \beta) \cos \theta \right] \left[\sum_{m=1}^{N_\xi} \sum_{n=1}^{N_\eta} A_{im}^\xi A_{jn}^\eta \varphi_{mn}^\xi \right] \tag{17}
 \end{aligned}$$

$$\begin{aligned}
 & - \left[2 \frac{Eh^3}{12} (\gamma \tan \theta - \mu) \right] \left[\sum_{m=1}^{N_\xi} \sum_{n=1}^{N_\eta} A_{im}^\xi A_{jn}^\eta \varphi_{mn}^\eta \right] - \left[\frac{Eh^3}{12} (\gamma \tan \theta - \mu) \right] \left[\sum_{n=1}^{N_\eta} B_{jn}^\eta \varphi_{in}^\xi \right] \\
 & - k^2 Gh \cos \theta \left[\varphi_{ij}^\eta - (\sin \theta) \varphi_{ij}^\xi - (\tan \theta) \sum_{m=1}^{N_\xi} A_{im}^\xi w_{mj} + (\sec \theta) \sum_{n=1}^{N_\eta} A_{jn}^\eta w_{in} \right] = 0,
 \end{aligned}$$

where $A_{ij}^\xi, A_{ij}^\eta, B_{ij}^\xi, B_{ij}^\eta, w_{ij}, \varphi_{ij}$ are the weighting coefficients of the first-order derivatives with respect to the variable of ξ and η , the weighting coefficients of the second-order derivatives with respect to the variable of ξ and η and deflection and rotation at grid point ij , respectively. The

boundary conditions in this study are shown in Appendix (A).

Now, the shear buckling coefficient λ_{xy} can be defined as

$$\lambda_{xy} = \frac{\tau_{xy} h b^2}{\pi^2 D}, \tag{18}$$

Table 2 Convergence of R-shear and S-shear buckling coefficient of SSSS and CCCC skew plates under various skew angles and thickness ratios with DT

B.C	Theories of plasticity	θ	h/b		$N_\xi = N_\eta$				
					7	9	11	13	15
SSSS	IT	45°	0.001	λ_R	9.6729	9.6633	9.6562	9.6535	9.6535
				λ_S	64.6871	62.8196	62.3847	62.3214	62.3214
			0.1	λ_R	6.7740	6.7128	6.6996	6.6956	6.6956
				λ_S	34.6736	34.2546	34.1616	34.1615	34.1615
CCCC	DT	−45°	0.001	λ_R	205.2209	44.6192	32.7628	31.3899	31.3898
				λ_S	19.9406	10.5069	9.3207	9.2563	9.2563
			0.1	λ_R	1.2562	1.1563	1.1343	1.1306	1.1306
				λ_S	1.0481	0.9992	0.9920	0.9920	0.9920

Table 3 Influence of skew angle on the accuracy and convergence of R-shear buckling coefficient of CCCC skew plates with DT ($h/b = 0.001$)

θ	$N_\xi = N_\eta$					
	7	9	11	13	15	17
15°	14.4650	14.3629	14.3540	14.3540	14.3540	14.3540
30°	16.7630	16.6034	16.5954	16.5953	16.5953	16.5953
45°	24.5933	24.0842	24.0409	24.0401	24.0401	24.0401
60°	55.9250	50.5452	46.0918	45.4138	45.4138	45.4138

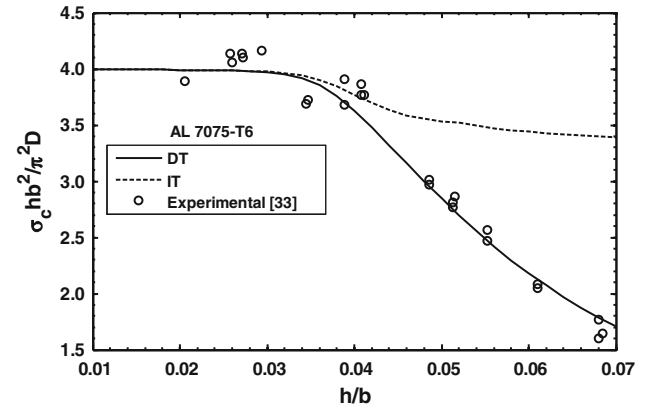


Fig. 3 Comparisons of buckling coefficients obtained by IT and DT with test results ($\theta = 0, a/b = 1$)

where $D = \frac{Eh^3}{12(1-\nu^2)}$ is the flexural rigidity. For R-shear loading (pure shear stress $\tau_{xy} = R$), we have

$$\lambda_{xy} = \lambda_R, \quad \lambda_x = \lambda_y = 0, \tag{19}$$

and for S-shear loading (shear stress $\tau_{xy} = S$ and uniaxial stress $\sigma_x = -2S \tan \theta$), we have

$$\lambda_{xy} = \lambda_S, \quad \lambda_x = -2\lambda_S \tan \theta, \tag{20}$$

where λ_R and λ_S are the elastic/plastic shear buckling coefficients for R- and S-shear loadings.

3 Convergence and accuracy studies

The final equations matrix is a set of nonlinear eigenvalue equations with the size of $3(N_\xi)^2 \times 3(N_\eta)^2$. By solving the generalized eigenvalue problem of Eqs. (15)–(17), the buckling coefficients (the lowest eigenvalue) are obtained. The grid points employed in the computations are showed in Appendix (B). A computer program EBSPSL (Elastic/plastic Buckling of Skew Plates under In-Plane Shear Loading) is developed based on the above-mentioned formulation, which is very quick and easy to generate elastic/plastic buckling coefficient of plate. The material used in this study is a typical aerospace aluminum alloy (AL 7075-T6). Here the Ramberg–Osgood elastic/plastic stress–strain relationship is used

$$\varepsilon = \frac{\sigma}{E} + \frac{k\sigma_0}{E} \left(\frac{\sigma}{\sigma_0} \right)^c, \tag{21}$$

where ε is the total effective strain and c and k are material parameters. The tangent and secant moduli used in equations are calculated as follow:

$$\frac{E}{T} = 1 + ck \left(\frac{\sigma}{\sigma_0} \right)^{c-1}, \quad \frac{E}{S} = 1 + k \left(\frac{\sigma}{\sigma_0} \right)^{c-1}, \quad (c > 1) \tag{22}$$

The characteristics of this metal is obtained by means of Eq. (21), $E/\sigma_0 = 150$, Ramberg–Osgood parameters $c = 9.2$ and $k = 3/7$, shear correction factor $\kappa^2 = 5/6$ and Poisson’s ratio $\nu = 0.33$ [23].

Table 1 represents the accuracy of grid point’s distribution. The analytical skew plate solutions given by Xiang et al. [16] are also listed in this table for comparison. The present results for skew plate are in close agreement with results of Eq. (B.5). Hence, Eq. (B.5) has a good accuracy of grid spacing.

Convergence studies of R- and S-shear buckling coefficients are carried out first for skew plate with SSSS and CCCC boundary conditions as shown in Table 2 to establish the minimum grid points required for obtaining

Table 4 Comparison of R-shear and S-shear buckling coefficients of CCCC skew plate ($a/b = 1$, $h/b = 0.001$)

Sources	Method	$\theta = 15^\circ$		$\theta = 30^\circ$		$\theta = 45^\circ$	
		λ_R	λ_S	λ_R	λ_S	λ_R	λ_S
Wittrick [11]	FEM	–	–	16.69	–	24.32	–
Argyris [12]	Double-Fourier	–	–	16.69	–	24.41	–
Durvasula [14]	Ritz	14.39	–	16.66	–	24.8	–
Xiang et al. [16]	Ritz	14.35	22.29	16.60	39.89	24.04	89.16
York [17]	Lagrangian multiplier	14.41	–	16.63	–	24.04	–
Hamada [18]	FEM	–	22.28	–	39.92	–	–
Fried and Schmitt [19]	FEM	–	22.13	–	39.64	–	88.73
Present study	GDQ	14.354	22.294	16.595	39.894	24.040	89.161

Table 5 Comparison of plastic pure shear buckling coefficients of SSSS square plate with DT

b/h	Ref. [25]	Ref. [26]	Present method
20	2.504	2.50	2.4896
30	4.92	4.91	4.9012
40	7.39	7.37	7.3651
60	9.31	9.31	9.3083
100	9.32	9.32	9.3208

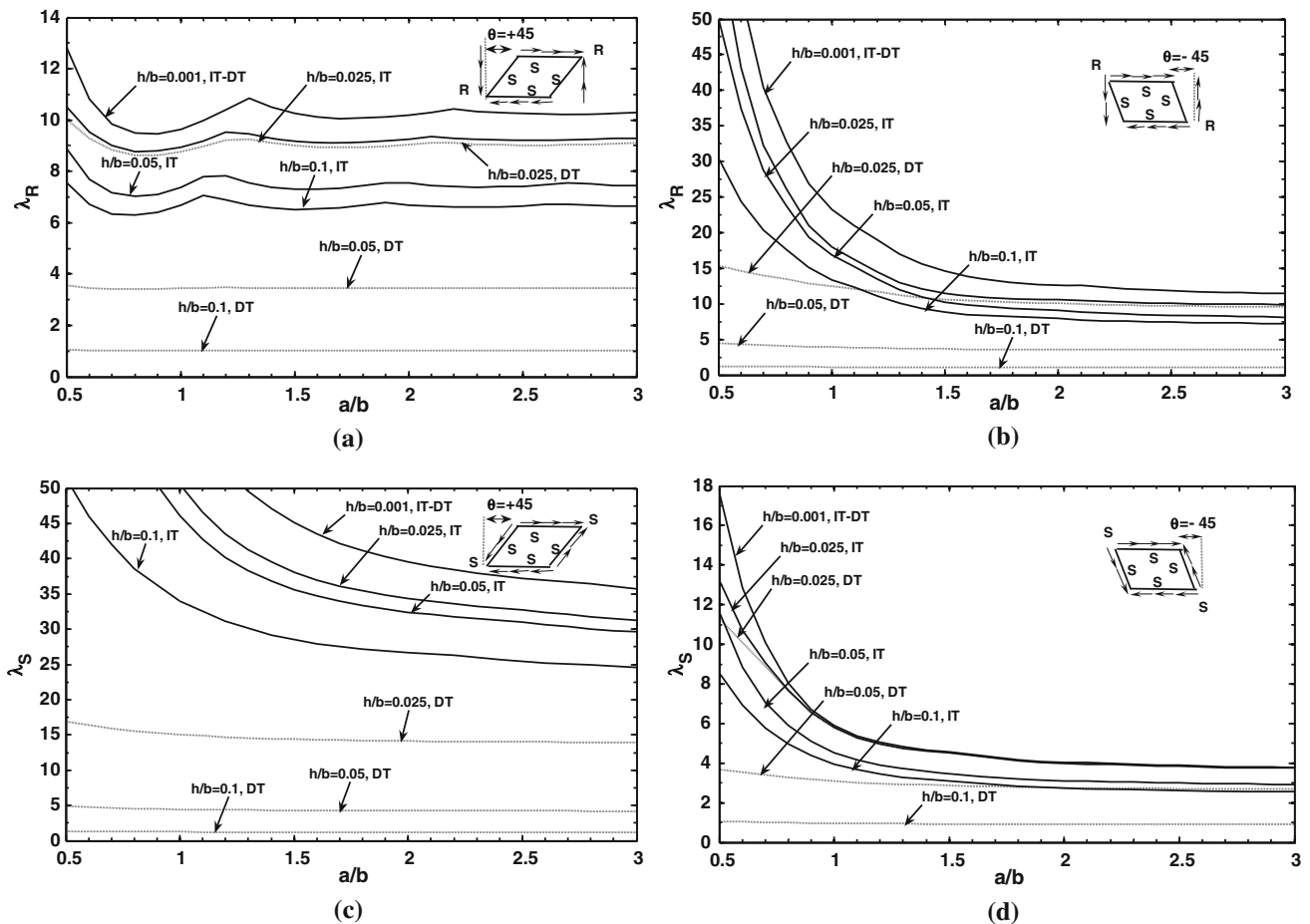


Fig. 4 The effects of aspect ratios on the R-shear and S-shear buckling coefficients of a SSSS skew plate for incremental and deformation theories and various thickness ratios

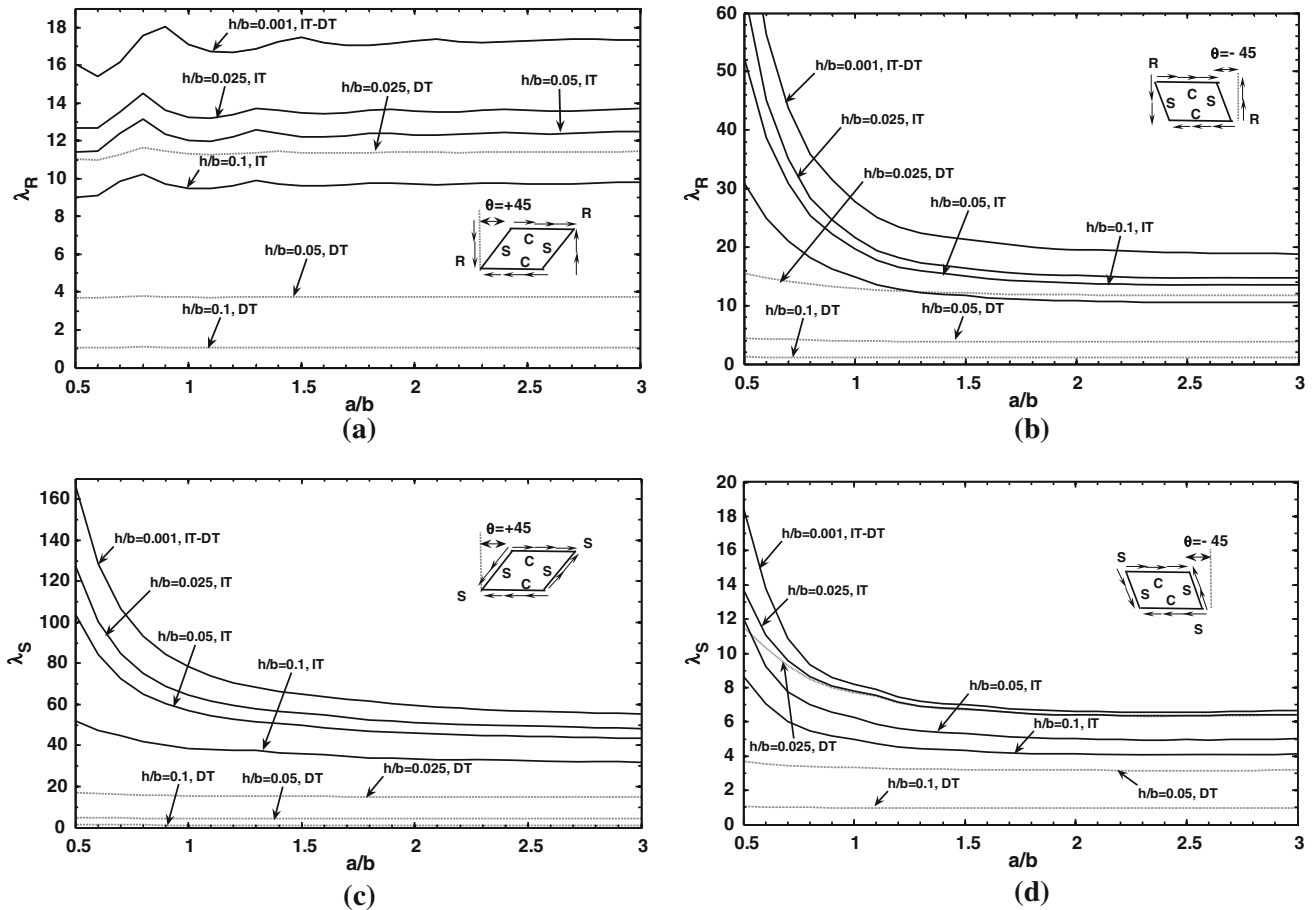


Fig. 5 The effects of aspect ratios on the R-shear and S-shear buckling coefficients of SCSC skew plate for incremental and deformation theories and various thickness ratios

accurate solutions. Two different values of thickness ratios and skew angles are considered. Previous experience showed that $N_\xi = N_\eta = N$ gave the best convergence rate [32]. From the data presented in Table 2, the fast rate of convergence of the method is quite evident and it is noticeable that thirteen grid point ($N_\xi = N_\eta = 13$) is sufficient to obtain the accurate results. Moreover, in all cases for $N_\xi = N_\eta \geq 13$ no change in the results are visible. It is seen that the convergence rate of GDQ method is excellent. The convergence rate is found to be slower when the skew angle increases, Table 3. It is found that thirteen grid points can yield results with acceptable accuracy. Again, the fast rate of convergence of the method is evident. A comparison between the obtained results and experimental data showed that the results attained by deformation theory are close to the experimental ones, Fig. 3.

The elastic and plastic shear buckling coefficients are used here to validate the presented formulation and the efficiency of the solution method. The elastic shear buckling coefficients, λ_R and λ_S (by setting $S = T = E$) subjected to

different skew angles for CCCC skew plates are compared with the published experimental and numerical results in the literature, Table 4. It is seen that in all cases the results are in very good agreement with those of the other methods. Moreover, the plastic R-shear buckling coefficients obtained from the present approach with DT have been presented in Table 5 and are compared with those given by Lotfi et al. [25] obtained by spline finite strip method and Jaberzadeh et al. [26] obtained by the element-free Galerkin method. It is obviously found that the present results are in excellent agreement with spline finite strip and element-free Galerkin methods. It should be pointed out that the results of Jaberzadeh et al. [26] could be correct only for thin plates and pure shear buckling coefficient. However, they used the thin plate formulation for thicker plates, as well, which could cause some errors in their results. But, in the current study the elastic/plastic buckling of thick skew plate along with the deformation and incremental theories of plasticity are used. Moreover, two shear loading conditions contain R- and S-shear loadings are studied.

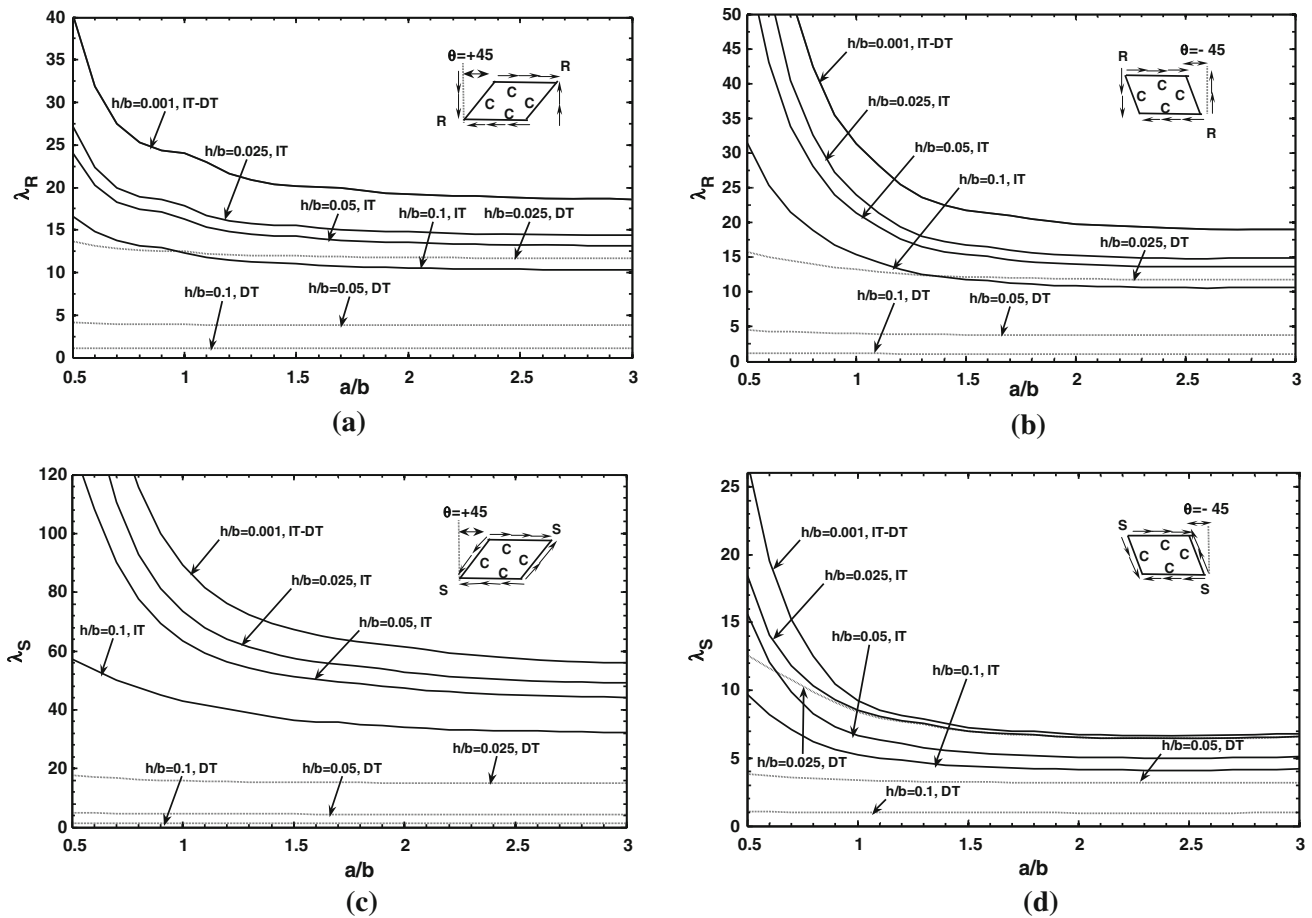
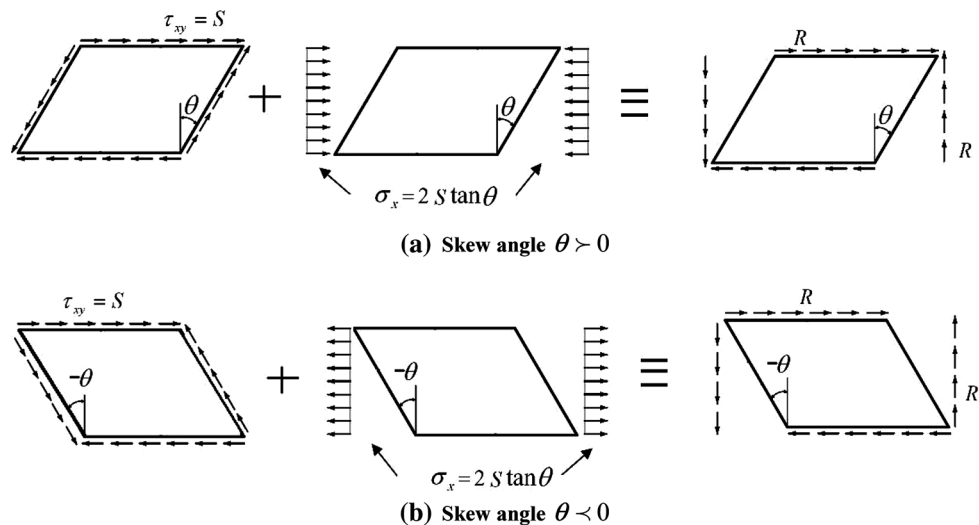


Fig. 6 The effects of aspect ratios on the R-shear and S-shear buckling coefficients of CCCC skew plate for incremental and deformation theories and various thickness ratios

Fig. 7 The relationships between R-shear loading and S-shear loading, $\theta > 0$ and $\theta < 0$



4 Numerical results and discussion

In this section, the effects of skew plate parameters such as aspect and thickness ratios, skew angle and boundary

condition on the shear buckling coefficients are comprehensively investigated in Figs. 4, 5, 6, 7, 8, 9, 10, 11, 12, 13 and 14. Finally, some mode shapes of the skew plates are shown in Figs. 15 and 16.

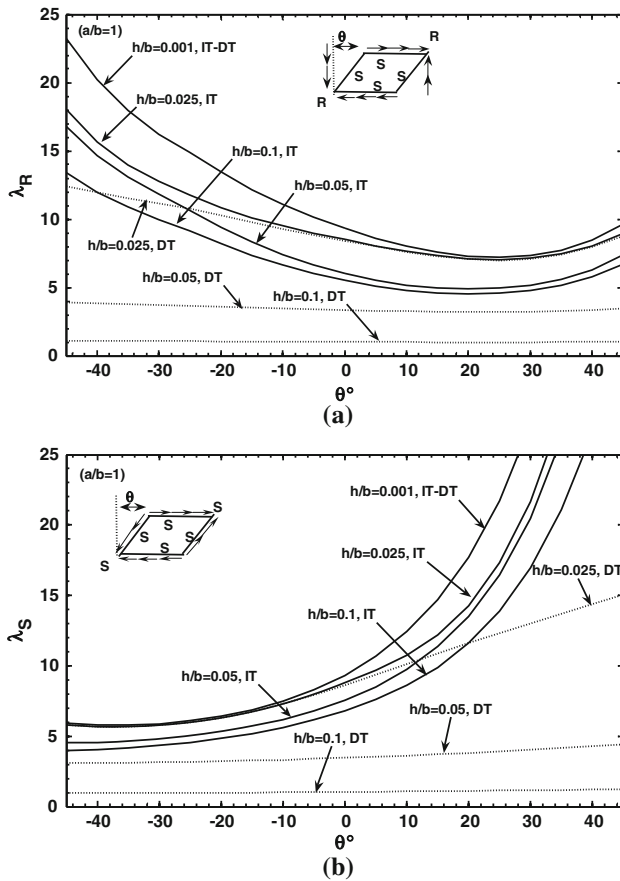


Fig. 8 The effects of skew angles on the R-shear and S-shear buckling coefficients of SSSS skew plate for incremental and deformation theories and various thickness ratios

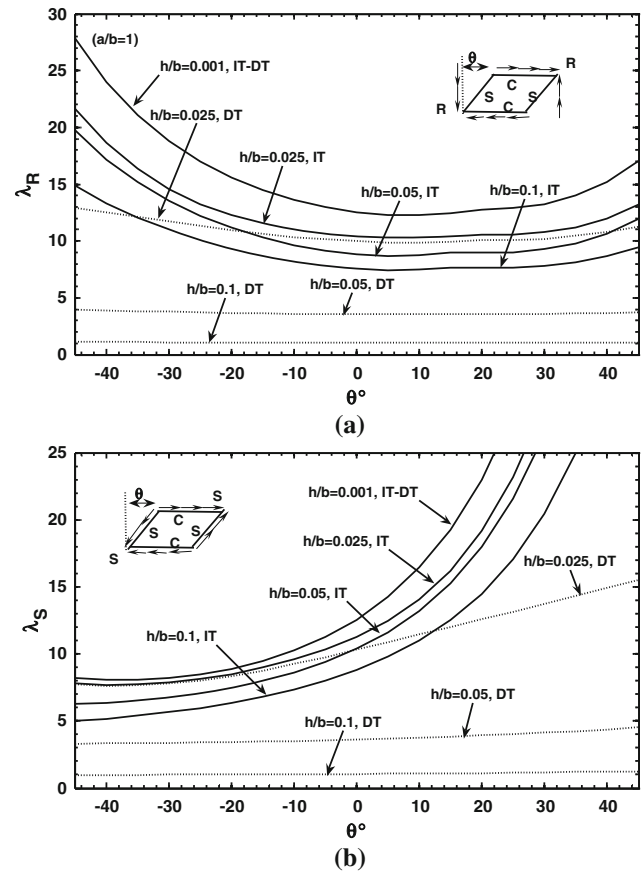


Fig. 9 The effects of skew angles on the R-shear and S-shear buckling coefficients of SCSC skew plate for incremental and deformation theories and various thickness ratios

4.1 Effect of aspect ratio on R- and S-shear buckling coefficients

The effects of aspect ratio for incremental and deformation theories and various thickness ratios on the R- and S-shear buckling coefficients, λ_R , λ_S of SSSS, SCSCS and CCCC skew plates are shown in Figs. 4, 5, and 6. Skew angles are $\theta = -45^\circ$ and $\theta = +45^\circ$ and the effect of both theories of plasticity on λ_R and λ_S are presented. In all figures, the R- and S-shear buckling coefficients predicted by IT and DT are shown by solid line and dash line, respectively. It can be seen that when the aspect ratio increases in the interval of $0.5 \leq a/b \leq 1.5$, the shear buckling coefficients decreases rapidly and for $1.5 < a/b \leq 3$, the buckling coefficient decreases monotonically. The R-shear and S-shear buckling coefficients have larger values when the skew angles are negative ($-\theta^\circ$) and positive ($+\theta^\circ$), respectively. This is due to the fact that in S-shear loading conditions, when $\theta < 0$ axial tension loading and when $\theta > 0$ axial compression loading are applied, Fig. 7. In rectangular plate $\theta = 0$ and therefore $\lambda_R = \lambda_S$. It is obvious from Figs. 4, 5 and 6, that the R- and S-shear buckling

coefficients decreases as the thickness ratio increases. For the smaller aspect ratios more reductions are observed. Moreover, the maximum discrepancy between incremental and deformation theories results occurs in R-shear buckling coefficient, λ_R , when $\theta < 0$ and in S-shear buckling coefficient, λ_S , when $\theta > 0$. It is also observed that there is no agreement between the incremental and deformation theories results for the thickness ratio of $h/b \geq 0.05$. With increasing the thickness ratio and decreasing the aspect ratio, the distinctions between the shear buckling coefficients obtained by two theories of plasticity increases. The maximum variations between the incremental and deformation theories results occur in S-shear buckling coefficient, λ_S for different thickness ratios and boundary conditions, when $\theta > 0$, Figs. 4c, 5c and 6c.

4.2 Effect of skew angle on R- and S-shear buckling coefficients

Skew angle is an important parameter that affects the buckling behavior of skew plates significantly. The effects of skew angle for incremental and deformation theories and

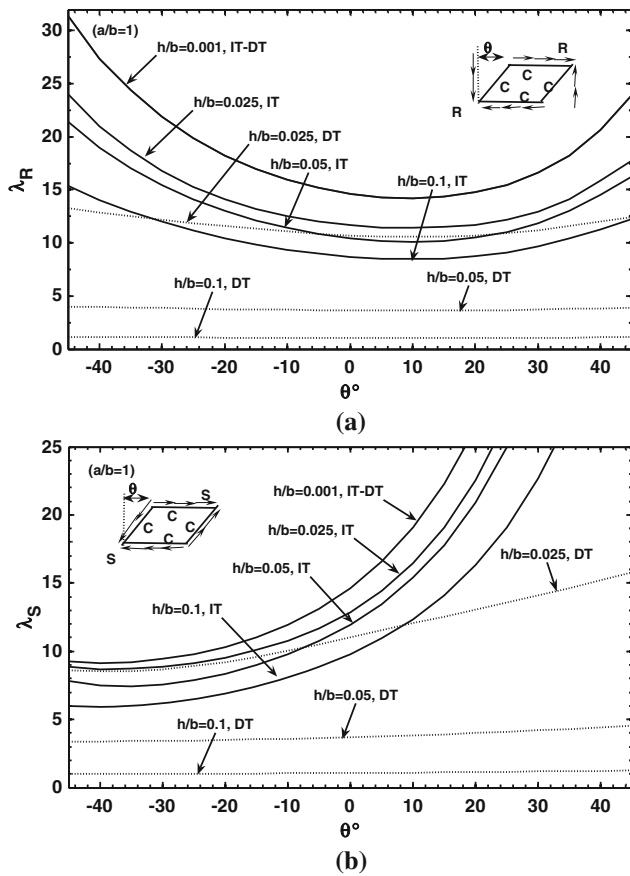


Fig. 10 The effects of skew angles on the R-shear and S-shear buckling coefficients of CCCC skew plate for incremental and deformation theories and various thickness ratios

various thickness ratios on the R- and S-shear buckling coefficients, λ_R and λ_S of SSSS, SCSCS and CCCC skew plates are illustrated in Figs. 8, 9 and 10. It is seen that the R-shear buckling coefficient initially decreases with increasing skew angle (from -45° to $+45^\circ$) and then increases as the skew angle increases. In the opposite skew angles ($-\theta^\circ$ and $+\theta^\circ$), the R-shear buckling coefficient is greater in negative skew angle ($\theta < 0$) for all cases which is more obvious for the incremental theory results. However, the S-shear buckling coefficient increases monotonically with increasing skew angle θ (from -45° to $+45^\circ$). With increasing the skew angle, the effect of transverse shear deformation on the S-shear buckling coefficient increases.

The deformation theory generally gives consistently lower shear buckling coefficients than incremental theory and large discrepancy between S-shear buckling coefficient, λ_S , from two theories with increasing the skew angle θ and thickness ratio is observed. This effect is more for λ_R and λ_S in negative and positive skew angles, respectively.

According to Figs. 8, 9 and 10, the R-shear buckling coefficients are about 2–3 times greater than those of S-shear buckling coefficient for $\theta = -45^\circ$ in all cases. On the other hand, for $\theta = +45^\circ$ the S-shear buckling coefficients are about 3–6 times greater than those of R-shear buckling. This is because the R-shear loading is equivalent to the S-shear loading plus a tensile uniaxial load when the skew angle is negative ($\theta < 0$) or plus a compressive uniaxial load when the skew angle is positive ($\theta > 0$), Fig. 7. Generally, it may be seen that the minimum R-shear buckling coefficient occurs in the interval of $0 < \theta < 30^\circ$ for various boundary conditions.

4.3 Effect of thickness ratio on R- and S-shear buckling coefficients

Figure 11 shows the variations of the shear buckling coefficients of SSSS skew plates versus thickness ratios and skew angles (for $\theta = +30^\circ$, $+45^\circ$ and $\theta = -30^\circ$, -45°). It is seen that with the increase of thickness ratio, shear buckling coefficients decrease, in all cases.

The shear buckling coefficients obtained from deformation theory have less dependency on skew angle, in all cases, Fig. 11. Moreover, the minimum variations between the incremental and deformation theories occur in S-shear buckling coefficient, λ_S , with negative skew angle, Fig. 11d.

Figures 12, 13 and 14 show the variations of shear buckling coefficients in various thickness ratios and positive and negative skew angles $\theta = +30^\circ$ and $\theta = -30^\circ$ and different boundary conditions. It is seen that with the increase of thickness ratio, the maximum discrepancy between the incremental and deformation theories results occurs in R-shear buckling coefficient in negative skew angle ($\theta = -30^\circ$) and S-shear buckling coefficient in positive skew angle ($\theta = +30^\circ$). For two opposite skew angles, the differences of buckling coefficients results obtained from deformation theory are much less than those of the incremental theory. Moreover, for the elastic buckling these differences are more than the other cases.

4.4 Effect of boundary conditions on R- and S-shear buckling coefficients

Generally, it can be seen from the figures that increasing the constraint at the edges of the skew plates increases the R- and S-shear buckling coefficients. Moreover, the transverse shear deformation causes more variations of buckling coefficient when more constraints applied on the edges of plate, Figs. 12, 13 and 14. In addition, the agreement between IT and DT results reduces with increasing the constraint at the edges of the skew plates.

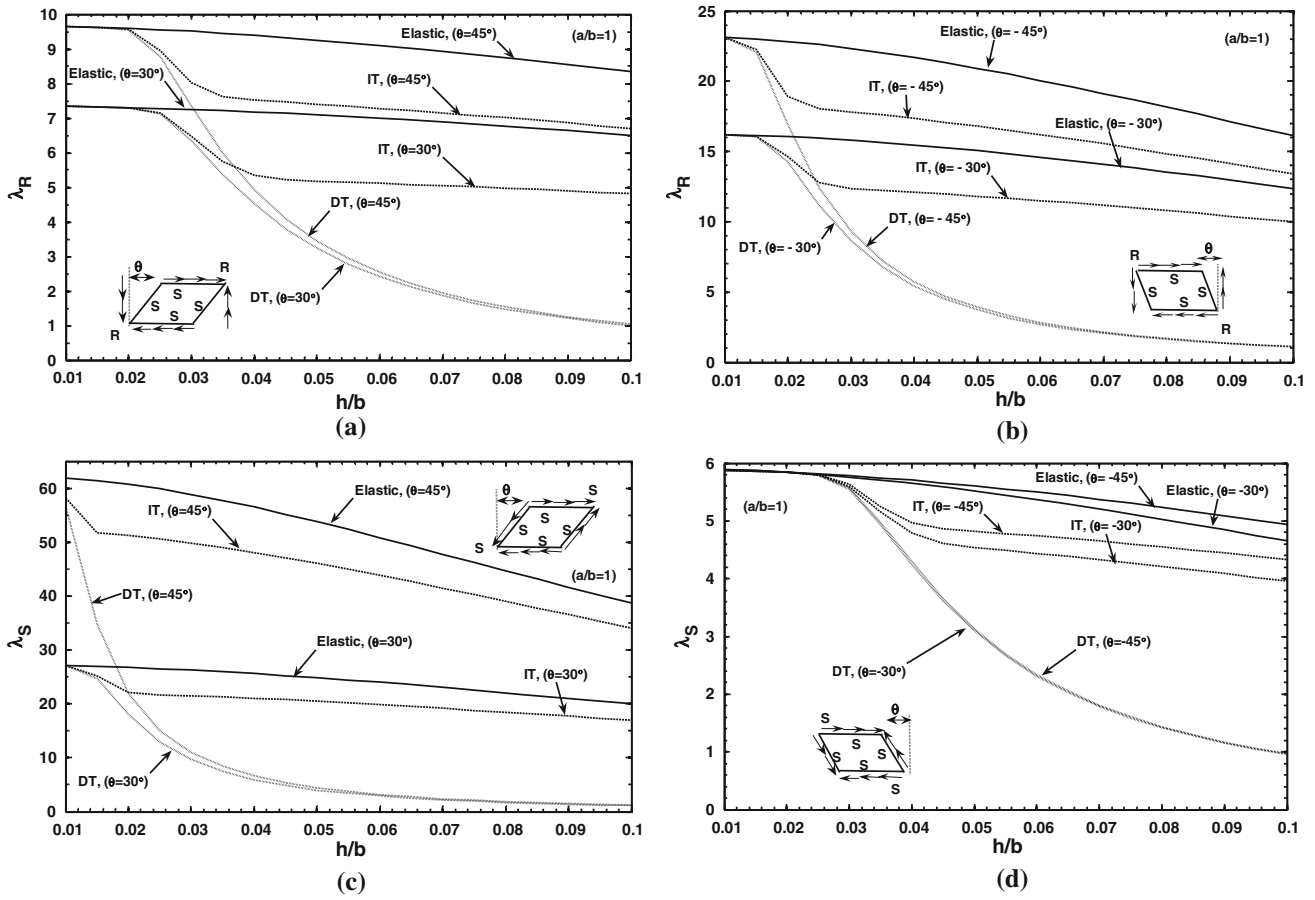


Fig. 11 The effects of thickness ratios on the R-shear and S-shear buckling coefficients of SSSS skew plate for incremental and deformation theories and various skew angles

4.5 Analysis of buckling mode shapes

Figures 15 and 16 show the buckling mode shapes for skew plates under various boundary conditions and aspect ratios for R- and S-shear loadings, respectively. It can be seen that the buckling mode shapes are different for R- and S-shear loadings when the same plate geometry is used. Moreover, it is observed that the buckling occurs in higher mode shapes as the aspect ratio increases which is more observable in R-shear buckling rather than in S-shear buckling, Figs. 4a, c, 15 and 16.

In R-shear loading under positive skew angle, $\theta = +45^\circ$, the number of half-sine waves in the shear buckling mode shape increases as the aspect ratio increases, Figs. 4a, 5a and 6a. Moreover, the locations of kinks are not the same for different plate thicknesses. For DT results, however, it is difficult to distinguish the location of kinks. For S-shear loading under positive skew angle, $\theta = +45^\circ$, the buckling coefficients decrease monotonically as the plate aspect ratio increases, Figs. 4c, 5c and 6c. Furthermore, these kinks locations depend on the plasticity

theories used. For example, the R-shear buckling mode contains three half-sine waves for IT rather than two half-sine waves for DT in SSSS skew plate for $h/b = 0.05$, $a/b = 2$ and $\theta = +45^\circ$, Figs. 4a and 15.

5 Conclusions

In this study, the equilibrium and stability equations for elastic/plastic buckling of skew plates under shear loading are obtained. Derivations are based on FSDT and incremental and deformation theories of plasticity. The governing equations are discretized via the generalized differential quadrature method as a simple and accurate numerical method and used for the first time to obtain the plastic R- and S-shear buckling coefficients. Closed form solutions for the R- and S-shear buckling coefficients are presented. The obtained results are compared with those obtained in the literature and good agreement is found. The effect of aspect and thickness ratios, skew angle, incremental and deformation theories and various boundary

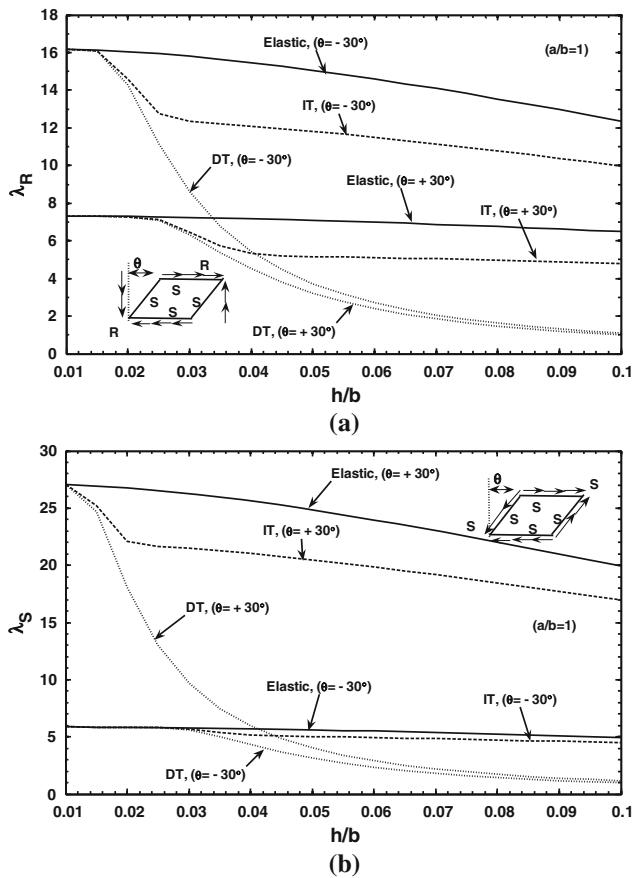


Fig. 12 The variations of shear buckling coefficients in various thickness ratios and skew angles of $\theta = +30^\circ$ and $\theta = -30^\circ$ for SSSS skew plate

conditions on the R- and S-shear buckling coefficients of the skew plate are investigated. Finally, plots of the mode shapes are given for R- and S-shear loadings with different boundary conditions and aspect ratios. Based on the numerical results, the following conclusions are reached:

- The discrepancy between IT and DT results for shear buckling coefficients increases with decreasing the aspect ratio and increasing the thickness ratio, constraint at the edges of skew plate and skew angle.
- In the opposite skew angles, the R- and S-shear buckling coefficients are greater in negative ($\theta < 0$) and positive ($\theta > 0$) skew angles, respectively.
- The S-shear buckling coefficient increase as the skew angle increases (from $-\theta^\circ$ to $+\theta^\circ$). However, the R-shear buckling coefficient initially increases and then decreases.
- The DT is more sensitive to thickness ratio than IT. Moreover, with increasing the thickness ratio it is more likely that plastic buckling take places than elastic one. On the other hand, more plasticity occurs in thicker

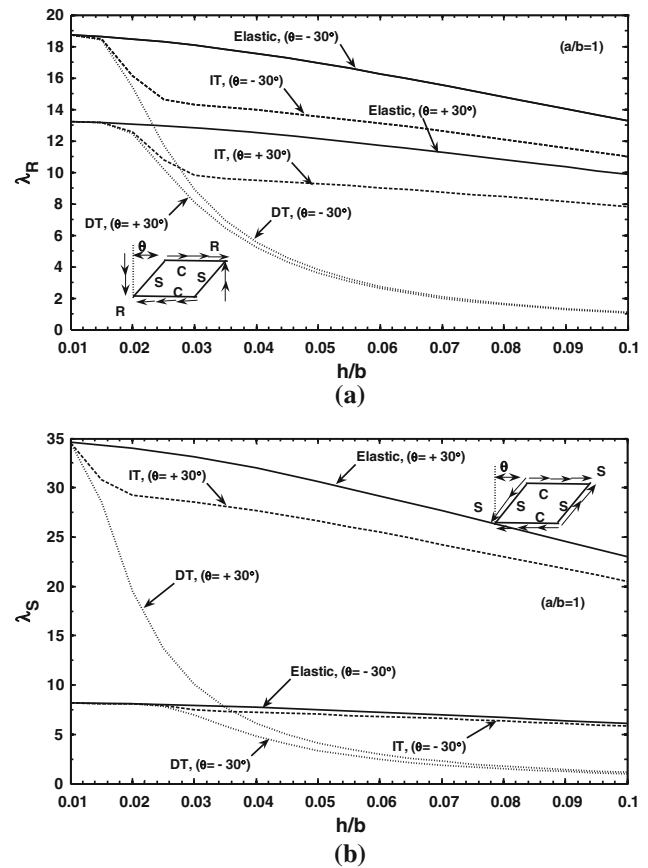


Fig. 13 The variations of shear buckling coefficients in various thickness ratios and skew angles of $\theta = +30^\circ$ and $\theta = -30^\circ$ for CSCS skew plate

plates which cause more discrepancy between IT and DT results. Furthermore, with increasing the thickness ratio, the results of the IT stand out of stress–strain curve gradually which shows this theory predicts invalid data.

- The maximum discrepancy between the incremental and deformation theories results occurs in R-shear buckling coefficient when $\theta < 0$ and S-shear buckling coefficient when $\theta > 0$.
- In the shear buckling of skew plates the deformation theory generally gives consistently lower shear buckling coefficients than those of the incremental theory.
- For the negative skew angles, the R-shear buckling coefficients are greater than those of S-shear ones and for the positive skew angles it is vice versa.
- The variations of buckling mode shapes depend on the type of plasticity theory used.

The authors believe that the presented GDQ solutions for plastic R- and S-shear buckling solutions of skew plates are valuable as they may serve as benchmark results for future researchers in this area.

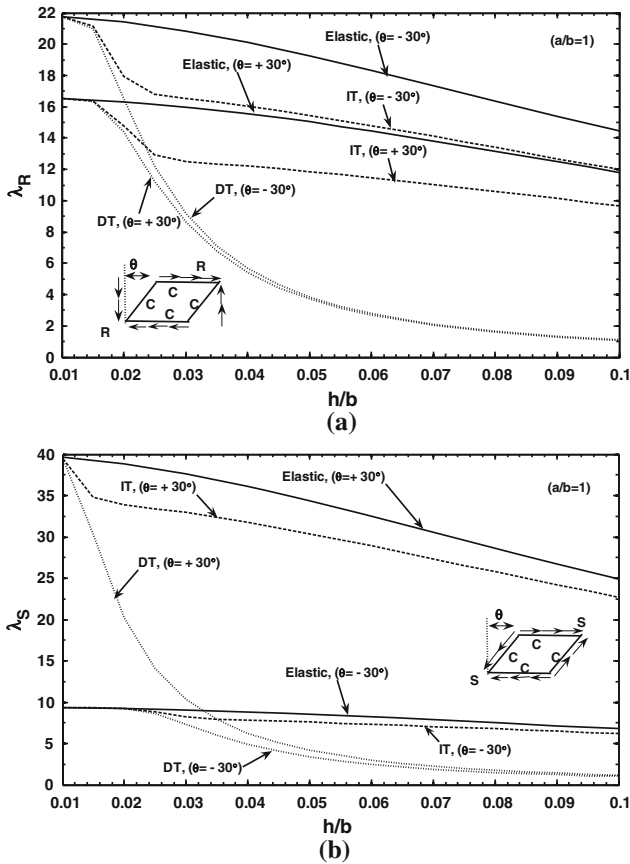


Fig. 14 The variations of shear buckling coefficients in various thickness ratios and skew angles of $\theta = +30^\circ$ and $\theta = -30^\circ$ for CCCC skew plate

Appendix (A): The boundary conditions in this study

(a) Clamped edge (C)

– for $\xi = 0$ and $\xi = a$

$$w_{1j} = w_{N_\xi j} = 0, \quad \varphi_{1j}^\xi = \varphi_{N_\xi j}^\xi = 0,$$

$$\varphi_{1j}^\eta = \varphi_{N_\xi j}^\eta = 0, \quad j = 1, \theta, \dots, N_\eta. \quad (A.1)$$

– for $\eta = 0$ and $\eta = b$

$$w_{i1} = w_{iN_\eta} = 0, \quad \varphi_{i1}^\xi = \varphi_{iN_\eta}^\xi = 0,$$

$$\varphi_{i1}^\eta = \varphi_{iN_\eta}^\eta = 0, \quad i = 1, \dots, N_\xi. \quad (A.2)$$

(b) Simply supported edge (S)

– for $\xi = 0$ and $\xi = a$

$$w_{1j} = w_{N_\xi j} = 0, \quad \varphi_{1j}^\eta = \varphi_{N_\xi j}^\eta = 0,$$

$$i = 1, \dots, N_\xi, \quad j = 1, \dots, N_\eta.$$

$$(\alpha \cos^2(\theta) + \beta \sin^2(\theta)) \sum_{m=1}^{N_\xi} A_{im}^\xi \varphi_{mj}^\xi - \beta \sin(\theta)$$

$$\left(\sum_{m=1}^{N_\xi} A_{im}^\xi \varphi_{mj}^\eta + \sum_{n=1}^{N_\eta} A_{jn}^\eta \varphi_{in}^\xi \right) + \beta \sum_{n=1}^{N_\eta} A_{jn}^\eta \varphi_{in}^\eta = 0, \quad (A.3)$$

– for $\eta = 0$ and $\eta = b$

$$w_{i1} = w_{iN_\eta} = 0, \quad \varphi_{i1}^\xi = \varphi_{iN_\eta}^\xi = 0,$$

$$i = 1, \dots, N_\xi, \quad j = 1, \dots, N_\eta.$$

$$(\beta \cos^2(\theta) + \gamma \sin^2(\theta)) \sum_{m=1}^{N_\xi} A_{im}^\xi \varphi_{mj}^\xi - \gamma \sin(\theta)$$

$$\left(\sum_{m=1}^{N_\xi} A_{im}^\xi \varphi_{mj}^\eta + \sum_{n=1}^{N_\eta} A_{jn}^\eta \varphi_{in}^\xi \right) + \gamma \sum_{n=1}^{N_\eta} A_{jn}^\eta \varphi_{in}^\eta = 0. \quad (A.4)$$

Appendix (B): The grid points employed in the computations are designed as follow: [30]

$$\xi_i = -\cos\left(\frac{i-1}{N_\xi-1}\pi\right), \quad i = 1, 2, \dots, N_\xi. \quad (B.1)$$

$$\xi_i = \frac{1}{2} \left(1 - \cos\left(\frac{i-1}{N_\xi-3}\pi\right) \right), \quad i = 3, \dots, N_\xi - 2. \quad (B.2)$$

$$\xi_i = \frac{1}{2} \left(1 - \cos\left(\frac{i-2}{N_\xi-3}\pi\right) \right), \quad i = 1, 2, \dots, N_\xi. \quad (B.3)$$

$$\xi_i = \frac{1}{2} \left(1 - \cos\left(\frac{2i-1}{2N_\xi}\pi\right) \right), \quad i = 1, 2, \dots, N_\xi. \quad (B.4)$$

The distributions of grid spacing of Chebyshev–Gauss–Lobatto (C-G-L) have the best convergence and highest accuracy [31, 32]. In this study, the following relation is used

$$\xi_i = \frac{1}{2} \left(1 - \cos\left(\frac{i-1}{N_\xi-1}\pi\right) \right), \quad i = 1, 2, \dots, N_\xi.$$

$$\eta_j = \frac{1}{2} \left(1 - \cos\left(\frac{j-1}{N_\eta-1}\pi\right) \right), \quad j = 1, 2, \dots, N_\eta. \quad (B.5)$$

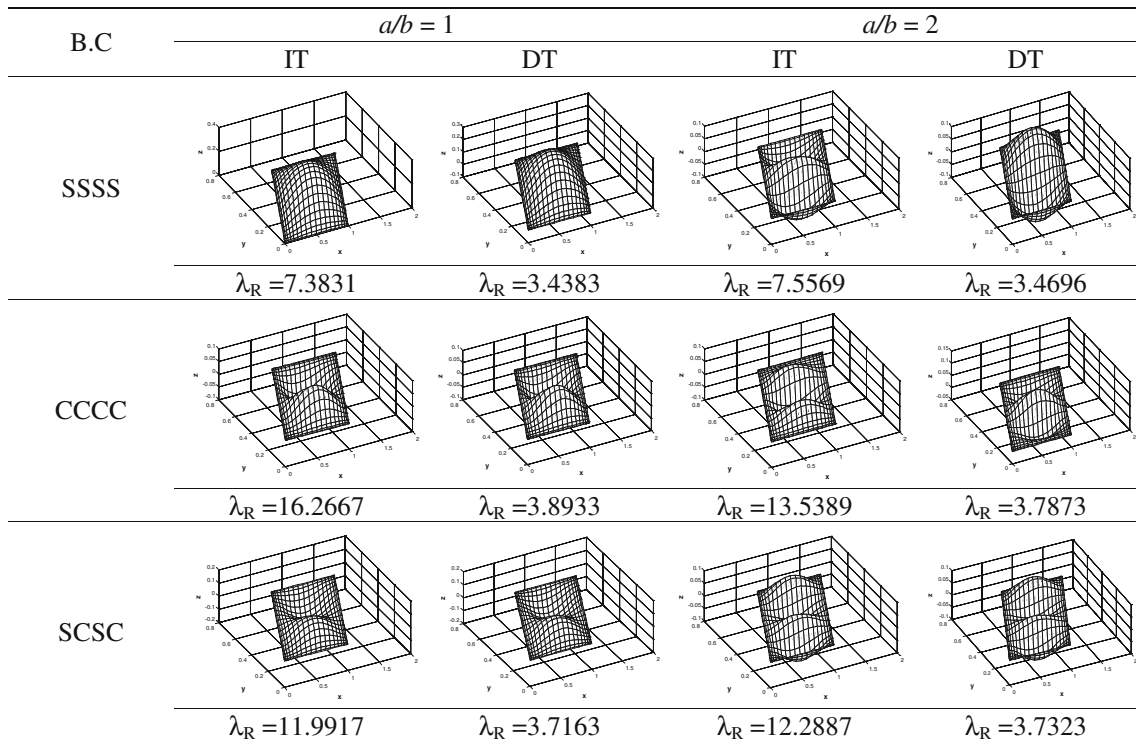


Fig. 15 Buckling mode shapes for skew plates under various boundary conditions on the R-shear buckling coefficient, λ_R ($h/b = 0.05$, $\theta = +45^\circ$)

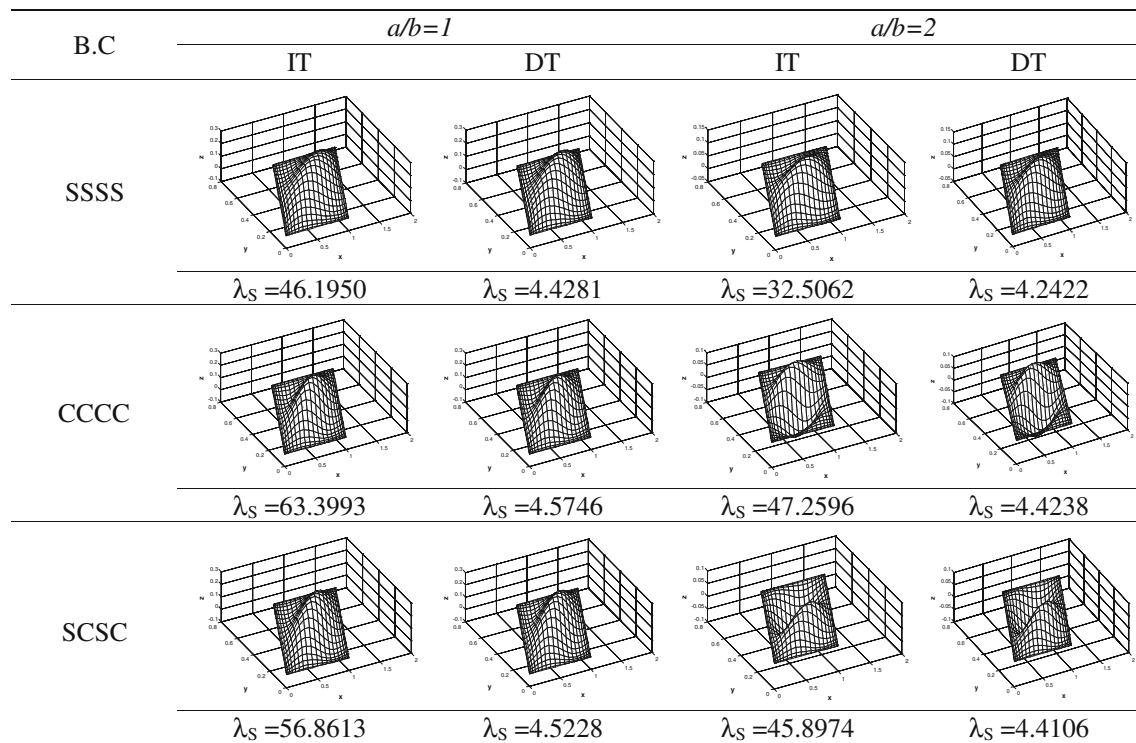


Fig. 16 Buckling mode shapes for skew plates under various boundary conditions on the R-shear buckling coefficient, λ_S ($h/b = 0.05$, $\theta = +45^\circ$)

References

1. Mizusawa T, Kajita T, Naruoka M (1980) Buckling of skew plate structures using B-spline functions. *Int J Numer Methods Eng* 15:87–96
2. Kitipomchai S, Xiang L, Wang CM, Liew KM (1993) Buckling of thick skew plates. *Int J Numer Methods Eng* 36(8):1299–1310
3. Wu WX, Shu C, Wang CM, Xiang Y (2010) Free vibration and buckling analysis of highly skewed plates least squares-based finite difference method. *Int J Struct Stab Dyn* 10:225–252
4. Zhang W, Wang X (2011) Elastoplastic buckling analysis of thick rectangular plates by using the differential quadrature method. *Comput Math Appl* 61:44–61
5. Xia P, Long SY, Wei KX (2011) An analysis for the elasto-plastic problem of the moderately thick plate using the meshless local Petrov-Galerkin method. *Eng Anal Bound Elem* 35:908–914
6. Fallah N, Parayandeh-Shahrestany A (2014) A novel finite volume based formulation for the elasto-plastic analysis of plates. *Thin-Walled Struct* 77:153–164
7. Belinha J, Dinis LMJS (2006) Elasto-plastic analysis of plates by the element free Galerkin method. *Eng Comput* 23:525–551
8. Belinha J, Dinis LMJS (2007) Nonlinear analysis of plates and laminates using the element free Galerkin method. *Compos Struct* 78:337–350
9. Kadkhodayan M, Maarefdoust M (2014) Elastic/plastic buckling of isotropic thin plates subjected to uniform and linearly varying in-plane loading using incremental and deformation theories. *Aerosp Sci Technol* 32:66–83
10. Morley LSD (1963) *Skew plates and structures*. Pergamon, Oxford
11. Wittrick WH (1954) Buckling of oblique plates with clamped edges under uniform shear. *Aeronaut Q* 5:39–51
12. Argyris JH (1965) Continua and discontinua. In: *Proceedings of the conference on matrix methods in structural mechanics*, Air Force Flight Dynamics Lab., AFFDL-TR, pp. 66–80
13. Ashton J (1969) Stability of clamped skew plates under combined loads. *J Appl Mech* 36:139–140
14. Durvasula S (1970) Buckling of clamped skew plates. *AIAA J* 8:178–181
15. Durvasula S (1971) Buckling of simply supported skew plates. In: *Proceedings of the ASCE, J. EM Division*, 97, pp 967–979
16. Xiang Y, Wang CM, Kitipornchai S (1995) Buckling of skew Mindlin plates subjected to in-plane shear loadings. *Int J Mech Sci* 37:1089–1101
17. York CB (1996) Influence of continuity and aspect ratio on the buckling of skew plates and assemblies. *Int J Solids Struct* 33:2133–2159
18. Hamada M (1959) Compressive or shearing buckling load and fundamental frequency of a rhomboidal plate with all edges clamped. *Bulletin of JSME* 2(8):520–526
19. Fried I, Schmitt KH (1972) Numerical results from the application of gradient iterative techniques to the finite element vibration and stability analysis of skew plates. *Aeronaut J* 76:166–169
20. Yoshimura Y, Iwata K (1963) Buckling of simply supported oblique plates. *J Appl Mech* 30:363–366
21. Durban D (1998) Plastic buckling of plates and shells. *AIAA Paper 97-1245 NACA/CP 206280:293–310*
22. Durban D, Zuckerman Z (1999) Elastoplastic buckling of rectangular plates in biaxial compression/tension. *Int J Mech Sci* 41:751–765
23. Wang CM, Xiang Y, Chakrabarty J (2001) Elastic/plastic buckling of thick plates. *Int J Solids Struct* 38:8617–8640
24. Wang CM, Aung TM (2007) Plastic buckling analysis of thick plates using p-Ritz method. *Int J Solids Struct* 44:6239–6255
25. Lotfi S, Azhari M, Heidarpour A (2011) Inelastic initial local buckling of skew thin thickness-tapered plates with and without intermediate supports using the isoparametric spline finite strip method. *Thin-Walled Struct* 49:1475–1482
26. Jaberzadeh E, Azhari M, Boroomand B (2013) Inelastic buckling of skew and rhombic thin thickness-tapered plates with and without intermediate supports using the element-free Galerkin method. *Appl Math Model* 37:6838–6854
27. Bellman RE, Casti J (1971) Differential quadrature and long-term integration. *J Math Anal Appl* 34:235–238
28. Bert CW, Malik M (1996) *Differential quadrature method in computational mechanics: a review*, ASME. *Appl Mech Rev* 49:1–28
29. Wu TY, Liu GR (1999) A differential quadrature as a numerical method to solve differential equations. *Comput Mech* 24:197–205
30. Shu C (2000) *Differential quadrature and its application in engineering*. Springer, New York
31. Shu C, Richards BE (1992) Application of generalized differential quadrature to solve two-dimensional incompressible Navier Stokes equations. *Int J Numer Methods Fluids* 15:791–798
32. Shu C, Chen H, Du Xue H (2001) Numerical study of grid distribution effect on accuracy of DQ analysis of beams and plates by error estimation of derivative approximation. *Int J Numer Methods Eng* 51:159–179
33. Anderson RA, Anderson (1956) Correlation of crippling strength of plate structures with material properties. *NACA Technical Note 3600*, Washington DC